Measurements of four-jet differential cross sections in $\sqrt{s} = 8$ TeV proton-proton collisions using the ATLAS detector

S Sacerdoti([1]) on behalf of the Atlas Collaboration

([1]) *Universidad de Buenos Aires - Buenos Aires, Argentina*

Summary. — Differential cross sections for the production of at least four jets have been measured in proton–proton collisions at $\sqrt{s} = 8$ TeV at the Large Hadron Collider using the ATLAS detector. Events are selected if the four anti-$k_t R = 0.4$ jets with the largest transverse momentum (p_{T}) within the rapidity range $|y| < 2.8$ are well separated ($\Delta R_{\mathrm{ij}} > 0.65$), all have $p_{\mathrm{T}} > 64$ GeV, and include at least one jet with $p_{\mathrm{T}} > 100$ GeV. The dataset corresponds to an integrated luminosity of $20.3\,\mathrm{fb}^{-1}$. The cross sections, corrected for detector effects, are compared to leading-order and next-to-leading-order calculations as a function of the jet momenta, invariant masses, minimum and maximum opening angles and other kinematic variables.

PACS 12.38.-t – Quantum chromodynamics.
PACS 13.85.-t – High-energy reactions, hadron-induced, Inelastic scattering in hadron-induced reactions.

1. – Introduction

The production of particle jets at hadron colliders such as the Large Hadron Collider (LHC) [1] provides a fertile testing ground for the theory describing strong interactions, Quantum Chromodynamics (QCD). In QCD, jet production is interpreted as the fragmentation of quarks and gluons produced in the scattering process followed by their subsequent hadronisation. At high transverse momenta (p_{T}) the scattering of partons can be calculated using perturbative QCD (pQCD) and experimental jet measurements are directly related to the scattering of quarks and gluons. The large cross sections for such processes allow for differential measurements in a wide kinematic range and stringent testing of the underlying theory.

The analysis presented in this contribution [2] studies events where at least four jets are produced in a hard-scatter process using data collected by the ATLAS experiment [3]. These events are of particular interest as the corresponding Feynman diagrams require several vertices even at leading-order (LO) in the strong coupling constant α_{S}. Differential cross sections for these events were studied as a function of a variety of kinematic and topological variables which include momenta, masses and angles. The variety of

kinematic regimes and topological distributions allow to test the validity of QCD calculations, including the parton shower approximation and the necessity of higher-order matrix element (ME) in Monte Carlo (MC) generators. Additionally, four-jet events represent a background to many other processes at hadron colliders. Hence, the predictive power of the QCD calculations, in particular their ability to reproduce the shapes of the distributions studied in this analysis, is of general interest.

The data sample used was taken during the period from March to December 2012 with the LHC operating at a pp centre-of-mass energy of $\sqrt{s} = 8$ TeV. The application of data-quality requirements results in an integrated luminosity of $20.3\,\mathrm{fb}^{-1}$.

2. – Analysis Strategy

2˙1. *Event Reconstruction and Selection.* – This measurement uses jets reconstructed with the anti-k_t algorithm with four-momentum recombination as implemented in the FastJet package. The radius parameter is $R = 0.4$. The jets were calibrated using in-situ methods.

Cross sections are calculated for events with at least four jets within the rapidity range $|y| < 2.8$. Out of those four jets, the leading one must have $p_{\mathrm{T}} > 100$ GeV, while the next three must have $p_{\mathrm{T}} > 64$ GeV. In addition, these four jets must be well separated from one another by $\Delta R_{\mathrm{ij}} > 0.65$, where $\Delta R_{\mathrm{ij}} = \min_{\substack{i,j\in[1,4]\\ i\neq j}}(\Delta R_{ij})$, and $\Delta R_{ij} = (|y_i - y_j|^2 + |\phi_i - \phi_j|^2)^{1/2}$. This set of criteria is also referred to as the 'inclusive analysis cuts', to differentiate them from the cases where additional requirements are made, for example on the invariant mass of the four leading jets.

The inclusive analysis cuts are mainly motivated by the triggers used to select events. Two of the triggers select events with at least four jets, while the remaining two select events with at least one jet at a higher p_{T} threshold. Events are split into the four non-overlapping kinematic regions shown in fig. 1, requiring at least four well-separated jets with varying p_{T} thresholds in order to apply the corresponding trigger. This ensures trigger efficiencies greater than 99% for any event passing the inclusive analysis cuts.

2˙2. *Cross-section definition.* – Cross sections are measured differentially as a function of the kinematic variables defined in table I; the list includes momentum variables, mass variables and angular variables. In all cases, the only jets used are the four leading ones in p_{T}. The observables were selected for their sensitivity to differences between different Monte Carlo models of QCD processes and their ability to describe the dynamics of the events. Different phase-space regions are probed by binning the variables in regions defined by a lower bound on $p_{\mathrm{T}}^{(1)}$ $m_{4\mathrm{j}}$or $\Delta y_{3\mathrm{j}}^{\mathrm{min}}$.

Each of the cross-section distributions were individually unfolded using the Bayesian Iterative method [4], with two iterations. This method corrects for migrations between bins, background events and detector inefficiencies. The unfolding matrix was built using `Pythia`, by matching events at reconstructed and particle level. The matching was performed at an event level, without applying any jet-by-jet spatial matching. The binning of the distributions was determined in order to achieve a bin-by-bin purity between 70 and 90% and a statistical uncertainty in data below 10%.

2˙3. *Theoretical Predictions.* – Monte Carlo samples are used to estimate experimental systematic uncertainties, deconvolve detector effects, and provide predictions to be compared with the data. The full list of generators is shown in table II.

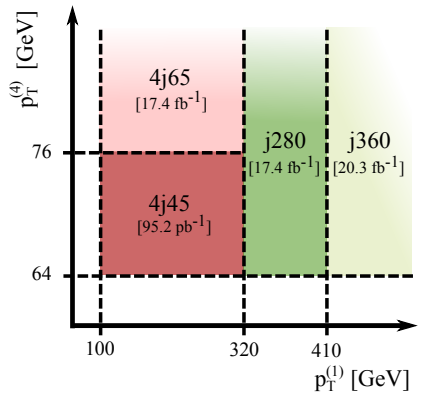

Figure 1. – Schematic of the kinematic regions in which the four different jet triggers are used, including the total luminosity that each of them recorded. The term 4j45 (4j65) refers to a trigger requiring at least four jets with $p_{\mathrm{T}} > 45$ GeV (65 GeV), where the p_{T} is measured at the EF level of the triggering system. The term j280 (j360) refers to a trigger requiring at least one jet with $p_{\mathrm{T}} > 280$ GeV (360 GeV) at the EF level. The horizontal and vertical axes correspond to $p_{\mathrm{T}}^{(1)}$ and $p_{\mathrm{T}}^{(4)}$ respectively, both calculated at the offline level (*i.e.*, including the full object calibration).

The samples used in the experimental studies comprise two LO $2 \to 2$ generators, `Pythia 8.160` and `Herwig++ 2.5.2`, and the LO multi-leg generator `Madgraph5 v1.5.12`. LO generators are still widely used in searches for new physics, which motivates the comparison of their predictions to the data. In addition, the results of the measurement are compared to two NLO predictions calculated using `BlackHat/Sherpa` and `NJet/Sherpa`, which are fixed-order calculations with no PS and no hadronisation. Lastly, the all order prediction `HEJ` was also compared to the measured results. The LO samples and `HEJ` were rescaled to facilitate the comparison with the data; the factors vary between 0.6 and 1.4. Not all generators describe the shape of $p_{\mathrm{T}}^{(1)}$ correctly, so these scale factors should not be seen as a measure of the level of agreement between MC simulation and data.

2˙4. *Uncertainties*. – The experimental uncertainties taken into account are the Jet Energy Scale (JES), Jet Energy Resolution (JER), Jet Angular Resolution (JAR) and the luminosity uncertainty. The dominating one is the JES, with a typical size between 4 and 15%.

In the unfolding procedure, the main uncertainty component comes from the different Monte Carlo descriptions of the particle- and reco-level association efficiency. It is mostly subdominant, with values of 2–10%.

The theoretical uncertainties (scale and PDF) were calculated for `NJet` and `HEJ` (although only `NJet`'s are shown in the result plots) by varying independently the renormalisation and factorisation scales by factors of $\sqrt{2}$, 2, $1/\sqrt{2}$ and $1/2$ around the central value of $H_{\mathrm{T}}/2$. The total uncertainty is the result of taking the envelope of all the variations. The uncertainty is found to be large, with values of $^{+50\%}_{-30\%}$.

Name	Definition	Comment
$p_{\mathrm{T}}^{(i)}$	Transverse momentum of the ith jet	Sorted descending in p_{T}
H_{T}	$\sum_{i=1}^{4} p_{\mathrm{T}}^{(i)}$	Scalar sum of the p_{T} of the four jets
$m_{4\mathrm{j}}$	$\left(\left(\sum_{i=1}^{4} E_i\right)^2 - \left(\sum_{i=1}^{4} \mathbf{p}_i\right)^2\right)^{1/2}$	Invariant mass of the four jets
$m_{2\mathrm{j}}^{\mathrm{min}}/m_{4\mathrm{j}}$	$\min_{\substack{i,j\in[1,4]\\ i\neq j}} \left((E_i+E_j)^2 - (\mathbf{p}_i+\mathbf{p}_j)^2\right)^{1/2} \,/\, m_{4\mathrm{j}}$	Minimum invariant mass of two jets relative to invariant mass of four jets
$\Delta\phi_{2\mathrm{j}}^{\mathrm{min}}$	$\min_{\substack{i,j\in[1,4]\\ i\neq j}} (\lvert\phi_i - \phi_j\rvert)$	Minimum azimuthal separation of two jets
$\Delta y_{2\mathrm{j}}^{\mathrm{min}}$	$\min_{\substack{i,j\in[1,4]\\ i\neq j}} (\lvert y_i - y_j\rvert)$	Minimum rapidity separation of two jets
$\Delta\phi_{3\mathrm{j}}^{\mathrm{min}}$	$\min_{\substack{i,j,k\in[1,4]\\ i\neq j\neq k}} (\lvert\phi_i - \phi_j\rvert + \lvert\phi_j - \phi_k\rvert)$	Minimum azimuthal separation between any three jets
$\Delta y_{3\mathrm{j}}^{\mathrm{min}}$	$\min_{\substack{i,j,k\in[1,4]\\ i\neq j\neq k}} (\lvert y_i - y_j\rvert + \lvert y_j - y_k\rvert)$	Minimum rapidity separation between any three jets
$\Delta y_{2\mathrm{j}}^{\mathrm{max}}$	$\Delta y_{ij}^{\mathrm{max}} = \max_{i,j\in[1,4]} (\lvert y_i - y_j\rvert)$	Maximum rapidity difference between two jets
$\Sigma p_{\mathrm{T}}^{\mathrm{central}}$	$\lvert p_{\mathrm{T}}^{c}\rvert + \lvert p_{\mathrm{T}}^{d}\rvert$	If $\Delta y_{2\mathrm{j}}^{\mathrm{max}}$ is defined by jets a and b, this is the scalar sum of the p_{T} of the other two jets, c and d ('central' jets)

TABLE I. – *Definitions of the various kinematic variables measured. In all cases, only the four jets with the largest p_T are considered.*

3. – Analysis Results

This analysis studies a long list of variables, shown in table I. Due to time and space constrains this contribution only shows four examples. The full extent of the analysis can be found in the original publication [2].

Momentum variables. The first and fourth leading jet p_{T} are presented in fig. 2 and 3. Part of the importance of these variables lies in their wide use in analyses, alone or as inputs to more complex observables. All the LO generators show a slope with respect to the data in the leading jet p_{T}, `Madgraph` being the only to present a positive slope in $p_{\mathrm{T}}^{(1)}$. Both `Pythia` and `Madgraph` describe $p_{\mathrm{T}}^{(4)}$ well, whereas `HEJ` and `Herwig++` overestimate the number of events with high values. `NJet/Sherpa` shows a similar trend at high $p_{\mathrm{T}}^{(4)}$, but the discrepancy is mostly covered by the theoretical uncertainties. The description could perhaps be improved by matching the calculations to parton showers.

Angular variables. Angular variables are able to test the description of events with small- and wide-angle radiation, and provide information on the global spatial distribution of the jets. The $\Delta\phi_{3\mathrm{j}}^{\mathrm{min}}$ spectrum is shown in fig. 4. The different $p_{\mathrm{T}}^{(1)}$ cuts change the spatial distribution of the events, such that at low $p_{\mathrm{T}}^{(1)}$ most events contain two jets recoiling

Name	Hard scattering + PS/UE	LO/NLO	PDF
Pythia 8	`Pythia 8` + `Pythia 8`	LO ($2 \to 2$)	`CT10`
Herwig++	`Herwig++` + `Herwig++`	LO ($2 \to 2$)	`CTEQ6L1`
MadGraph	`Madgraph` + `Pythia 6`	LO ($2 \to 4$)	`CTEQ6L1`
HEJ	`HEJ`†		`CT10`
BlackHat	`BlackHat/Sherpa`	NLO ($2 \to 4$)	`CT10`
NJet	`NJet/Sherpa`	NLO ($2 \to 4$)	`CT10`

TABLE II. – *The generators used for comparison against the data are listed, together with the parton distribution functions (PDFs), PS algorithms and underlying event (UE).* (†) *The* `HEJ` *sample is based on an approximation to all orders in* α_S.

against two, while at high $p_{\mathrm{T}}^{(1)}$ the events where one jet recoils against three dominate. In general, the description of the data improves as $p_{\mathrm{T}}^{(1)}$ increases. For `Pythia`, the number of events where one jet recoils against three (low $\Delta\phi_{3\mathrm{j}}^{\mathrm{min}}$) is significantly overestimated when $p_{\mathrm{T}}^{(1)}$ is low; as $p_{\mathrm{T}}^{(1)}$ increases, the agreement improves such that the $p_{\mathrm{T}}^{(1)} > 1000$ GeV region is very well described. `Madgraph`, `Herwig++` and `HEJ` are mostly in good agreement with data.

$\Sigma p_T^{central}$ *variables*. These variables set a minimum forward–backward rapidity interval and measure the total p_{T} of the central jets ($\Sigma p_{\mathrm{T}}^{\mathrm{central}}$). They were defined to test the framework of `HEJ`, which has been designed to describe events with two jets significantly

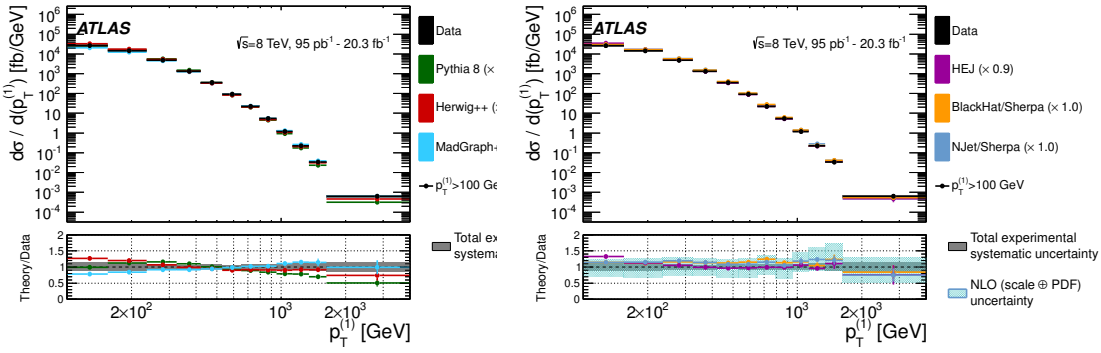

Figure 2. – The four-jet differential cross section as a function of leading jet $p_{\mathrm{T}}(p_{\mathrm{T}}^{(1)})$, compared to different theoretical predictions: `Pythia`, `Herwig++` and `Madgraph` (left), and `HEJ`, `NJet/Sherpa` and `BlackHat/Sherpa` (right), from ref. [2]. For better comparison, the predictions are multiplied by the factors indicated in the legend. In each figure, the top panel shows the full spectra and the bottom panel the ratios of the different predictions to the data. The solid band represents the total experimental systematic uncertainty centred at one. The patterned band represents the NLO scale and PDF uncertainties calculated from `NJet/Sherpa` centred at the nominal `NJet/Sherpa` values. The scale uncertainties for `HEJ` (not drawn) are typically $^{+50\%}_{-30\%}$. The ratio curves are formed by the central values with vertical uncertainty lines resulting from the propagation of the statistical uncertainties of the predictions and those of the unfolded data spectrum.

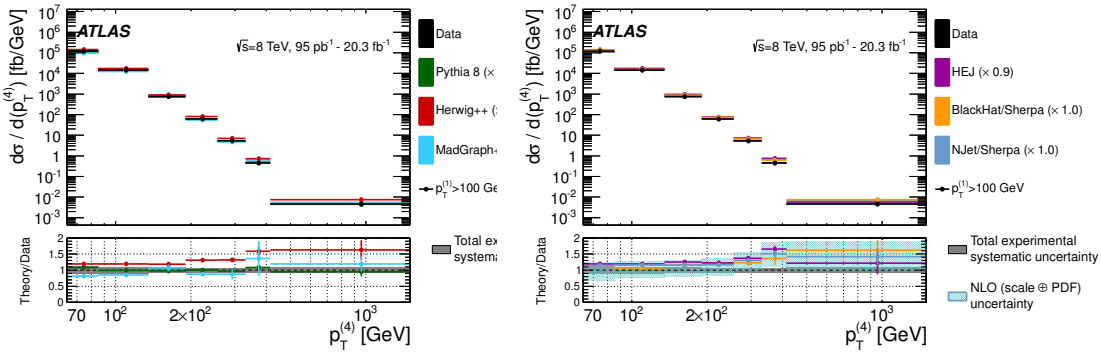

Figure 3. – Unfolded four-jet differential cross section as a function of $p_{\mathrm{T}}^{(4)}$, compared to different theoretical predictions, from ref. [2]. The other details are as for fig. 2.

separated in rapidity with additional, central, high-p_{T} radiation. The generators with $2 \to 2$ MEs have problems describing the data around the threshold values where the contribution from different jets changes, which results in kinks in the ratio distributions. One such transition occurs at the $\Sigma p_{\mathrm{T}}^{\mathrm{central}}$ value for which the leading jet is first allowed to be central. For $p_{\mathrm{T}}^{(1)} > 400$ GeV, this happens at $\Sigma p_{\mathrm{T}}^{\mathrm{central}} > 464$ GeV, at which point there is a major jump in `Pythia` in the second ratio plot of fig. 5. The discrepancies worsen for larger cuts in $\Delta y_{2\mathrm{j}}^{\mathrm{max}}$. `Madgraph` provides an excellent description of the $\Sigma p_{\mathrm{T}}^{\mathrm{central}}$ variables, especially at low $p_{\mathrm{T}}^{(1)}$. `HEJ` gives a good description of the high $\Sigma p_{\mathrm{T}}^{\mathrm{central}}$ region; while `NJet/Sherpa` has a tendency to overestimate the number of events with very low $\Sigma p_{\mathrm{T}}^{\mathrm{central}}$ but provides a good description otherwise.

4. – Conclusions

The NLO predictions, `BlackHat/Sherpa` and `NJet/Sherpa`, are almost always compatible with the data within their theoretical uncertainties, which are found to be large ($\mathcal{O}(30\%)$ at low momenta) and asymmetric. Within the normalisation scheme used, `Madgraph` also provides a good description of the data, as does `HEJ`, especially at high $p_{\mathrm{T}}^{(1)}$.

The description of the jet momenta is compatible with previous measurements of the multi-jet cross sections. `HEJ`, `NJet/Sherpa` and `BlackHat/Sherpa` give a very good description of the distributions of the leading jets but show some discrepancy with the data for $p_{\mathrm{T}}^{(4)}$. For variables that are particularly sensitive to wide-angle configurations and high-p_{T} radiation, such as masses or angles, `BlackHat/Sherpa`, `NJet/Sherpa` and `Madgraph` do a remarkable job overall. These measurements expose the shortcomings of $2 \to 2$ parton ME+PS predictions in a variety of scenarios and highlight the importance of the more sophisticated calculations.

REFERENCES

[1] Evans, (ed.), Lyndon and Bryant, (ed.), Philip, *JINST*, **3** (2008) S08001.
[2] The Atlas Collaboration, *JHEP*, **12** (2015) 105.
[3] The Atlas Collaboration, *JINST*, **3** (2008) S08003.
[4] D'Agostini, G., *Nucl. Instrum. Meth.*, **1995** (A362) 487.

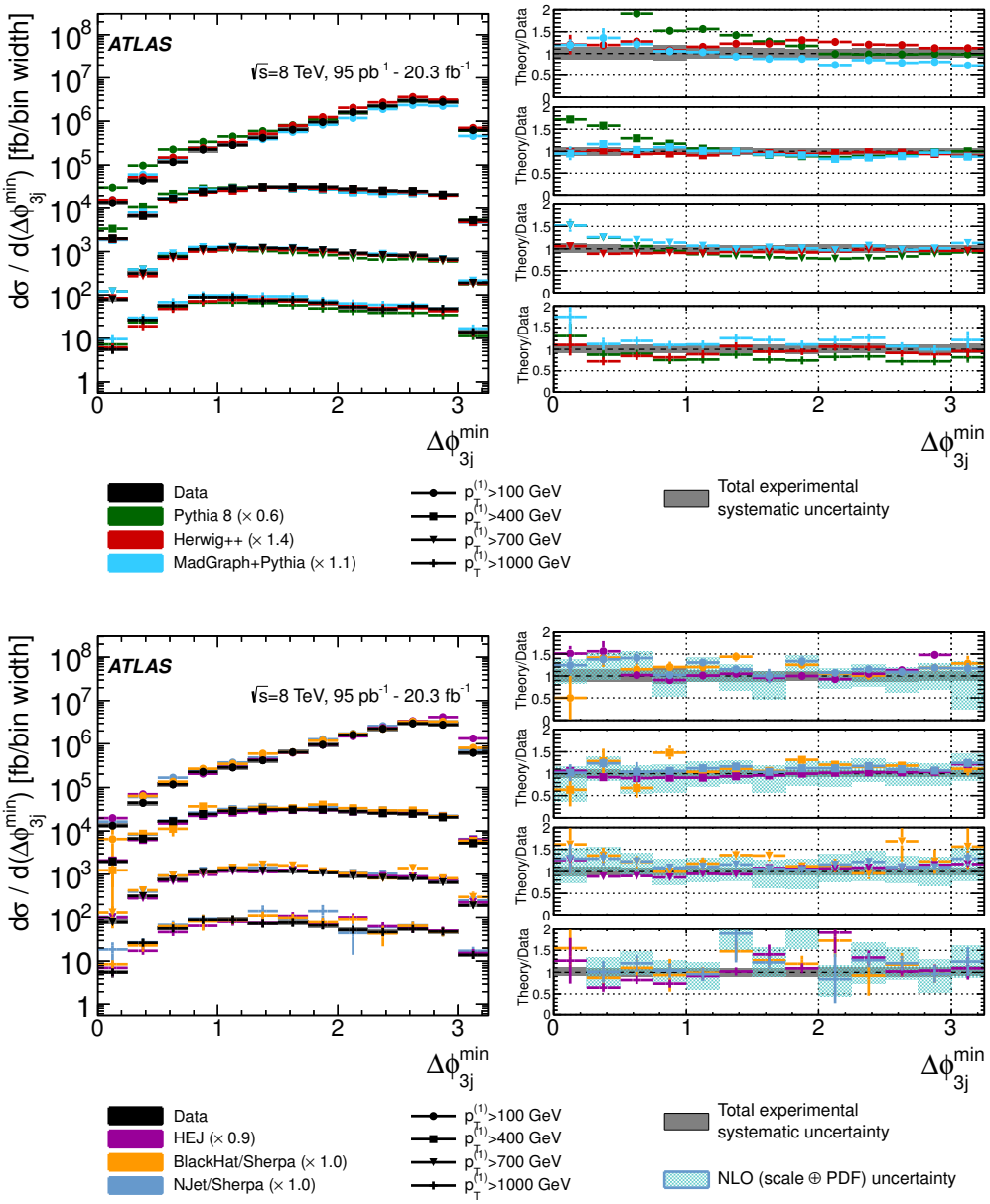

Figure 4. – Unfolded four-jet differential cross section as a function of $\Delta\phi_{3j}^{\min}$, compared to different theoretical predictions, from ref. [2]. In each figure, the left panel shows the full spectra and the right panel the ratios of the different predictions to the data, divided according to the selection criterion applied to $p_{\mathrm{T}}^{(1)}$. The other details are as for fig. 2. Some points in the ratio curves for `NJet/Sherpa` fall outside the y-axis range, and thus the NLO uncertainty is shown partially, or not shown, in these particular bins.

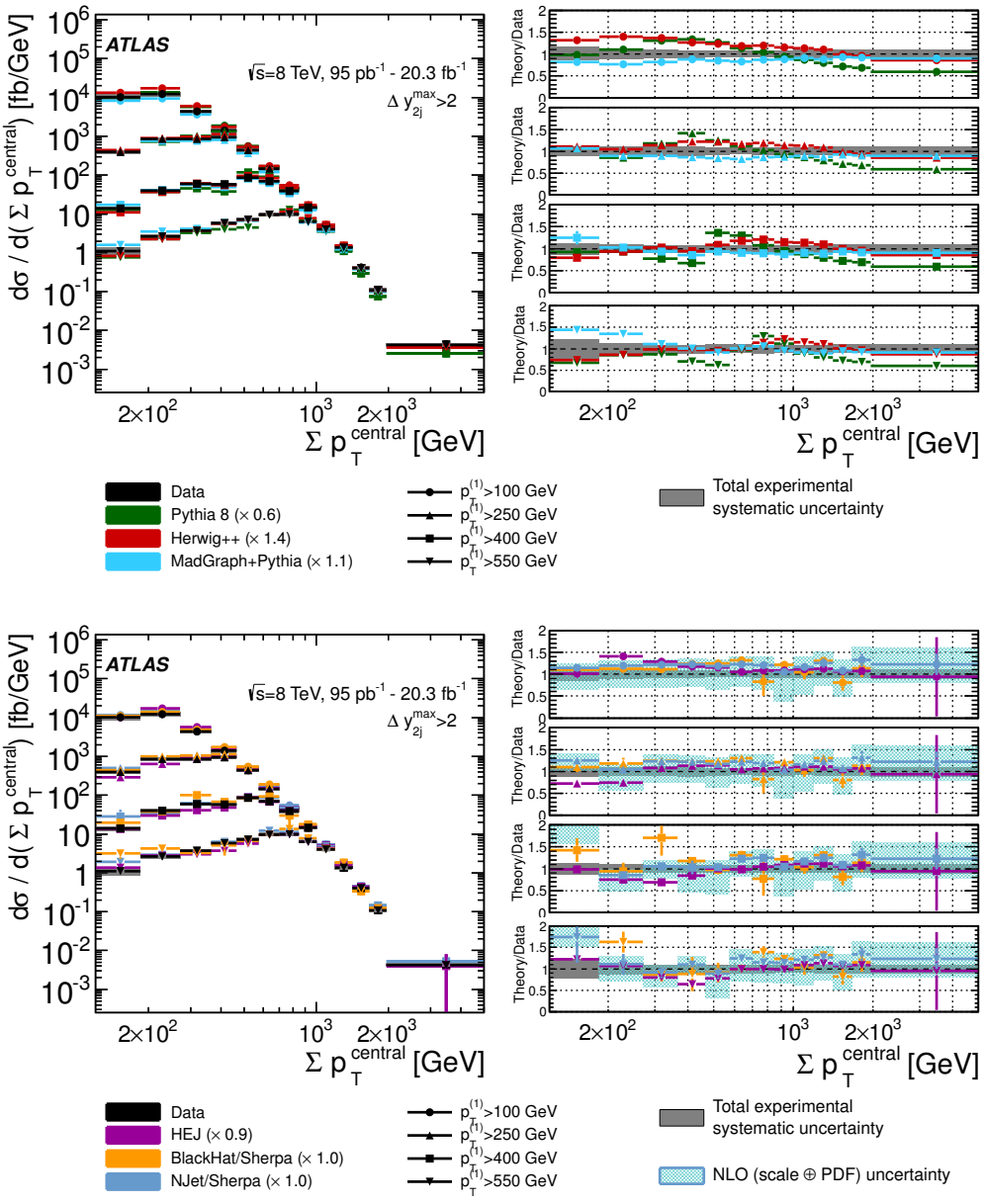

Figure 5. – Unfolded four-jet differential cross section as a function of $\Sigma p_{\mathrm{T}}^{\mathrm{central}}$ with $\Delta y_{2\mathrm{j}}^{\mathrm{max}} > 2$, compared to different theoretical predictions, from ref. [2]. The other details are as for fig. 4.